



Reactivation of the Adıyaman Fault (Turkey) through the Mw 5.7 2007 Sivrice earthquake: An oblique listric normal faulting within the Arabian-Anatolian plate boundary observed by InSAR



Selver Şentürk^{a,*}, Ziyadin Çakır^b, Semih Ergintav^c, Hayrullah Karabulut^c

^a Istanbul Technical University, Eurasia Institute of Earth Sciences, Istanbul, Turkey

^b Istanbul Technical University, Department of Geology, Istanbul, Turkey

^c Bogazici University, Kandilli Observatory and Earthquake Research Institute, Department of Geophysics, Istanbul, Turkey

ARTICLE INFO

Keywords:

InSAR
ENVISAT ASAR
Earthquakes
Sivrice
East Anatolian Fault
Adıyaman Fault
Listric fault

ABSTRACT

On February 21, 2007, a moderate-sized (Mw 5.7) earthquake struck the town of Sivrice (Elazığ, Turkey) located within the East Anatolian Fault (EAF) zone that forms the boundary between the Arabian and Anatolian plates. The earthquake source parameters of the mainshock reported by different agencies are significantly different. In the mean time, the relation of this earthquake to the EAF has not been fully explored. In this study, we combine remotely sensed Synthetic Aperture Radar data obtained from ENVISAT ASAR images (European Space Agency) with relocated seismicity to map the observed surface displacement field, resolve the earthquake source parameters and determine the fault plane geometry. We calculated coseismic interferograms from both ascending and descending orbits and modeled them by elastic dislocations on rectangular fault surfaces using a downhill simplex simulated annealing algorithm. InSAR analysis and seismicity distribution reveal that the earthquake took place on the Adıyaman fault (AF), a major southern splay of the EAF. The ruptured part of the AF has a listric geometry with an oblique normal slip (rake $-73 \pm 21^\circ$), and a strike of N42°E. The computed coseismic slip is 64 ± 18 cm with a moment magnitude of Mw 5.9. The resolved fault plane has a steep dip (greater than 80°) near the surface and mildly dipping at depths between 3.6 and 8.5 km (dip $63 \pm 4^\circ$). The kinematics of the faulting is supported by the observed transtensional left-lateral strike-slip regime in the region of tectonic depression of Hazar Lake.

1. Introduction

Assessing the earthquake hazard within major fault zones requires better understanding of the continental intraplate earthquakes and the distribution of their sources. Major transform faults like the EAF manifest a variety of geological characteristics over their expanse where the type of deformation can vary throughout. Nevertheless, describing the kinematics and structure of the EAF would be inadequate in the absence of accurate description of the neighboring tectonic units.

Large earthquakes are important as they give direct information on the general structure of a major fault. However, small to moderate sized earthquakes on subsidiary and intra-major faults are equally important as they complement this information with a clearer picture on the heterogeneities of the strain accumulation. Also, moderate sized earthquakes can still cause broad-scale property damage and casualties. The Ms 6.1 1995 Dinar, and the Mw 6.0 2000 Orta in Turkey or the Mw 6.6 2003 Bam in Iran earthquakes (Wright et al., 1999; Funning

et al., 2005; Çakır and Akoğlu, 2008) are some of the noteworthy examples.

The Mw 5.7 2007 Sivrice earthquake took place in the immediate vicinity of the EAF. An eastern Anatolian town, Sivrice is located within the young continental collision zone (McKenzie, 1972; Dewey and Şengör, 1979; Şengör, 1979), or more precisely on the southwestern tip of a lensoidal tectonic depression forming the Hazar Lake (upper Euphrates region). The quake caused extensive property damage in Sivrice and was reported from nearby and far districts such as Elazığ, Malatya, Adıyaman, Tunceli, and Diyarbakır. Field studies carried out in the vicinity and nearby villages indicate no apparent surface ruptures after the earthquake (Tepeuğur and Yaman, 2007). Nonetheless, the immediate location of Sivrice over a major fault, the high seismic intensity in the town and its villages led to preliminary inferences that the earthquake took place on the master Palu-Hazar-Sincik segment of the East Anatolian fault (EAF). Both the location and the focal mechanism solution of the earthquake provided by various local and global

* Corresponding author.

E-mail address: selsenturk@itu.edu.tr (S. Şentürk).

<https://doi.org/10.1016/j.jog.2019.101654>

Received 25 March 2019; Received in revised form 26 July 2019; Accepted 10 August 2019

Available online 14 August 2019

0264-3707/ © 2019 Elsevier Ltd. All rights reserved.

Table 1

Focal mechanism solutions provided for the Sivrice earthquake (<https://www.emsc-csem.org>). CGMT (Ekström et al., 2012), USGS (<https://earthquake.usgs.gov/earthquakes>), INGV (<http://cnt.rm.ingv.it/>), KOERI/KAN (<http://www.koeri.boun.edu.tr>), ETHZ (Swiss Seismological Service, 2008), ECOS02 (<http://www.seismo.ethz.ch>, July 2008), AFAD (<https://deprem.afad.gov.tr>), MAM (<http://ydbe.mam.tubitak.gov.tr/tr/veri-paylasimi>).

Source	Lon	Lat	Strike (°)	Dip (°)	Rake (°)	Mw
This study (InSAR)	39.3479	38.3533	222	59	-73	5.9
This study (seismology)	39.332	38.360	230	45	-59	5.7
GCMT	39.230	38.450	233	34	-38	5.7
USGS	39.275	38.318	232	35	-58	5.7
INGV	39.475	38.485	244	20	-6	5.9
KOERI	39.321	38.373	154	88	-170	5.7
ETHZ	39.242	38.341	274	60	60	5.9
AFAD	39.308	38.383	262	60	169	5.4
MAM	39.298	38.396	231	29	-58	5.7

agencies show significant differences from each other (Table 1).

Using SAR interferometry, we re-evaluate the location, mechanism and the causative fault of the moderate-sized Mw 5.7 2007 Sivrice

earthquake (Fig. 1). As a remote sensing technique, InSAR has the ability to illuminate the place of deformation in the absence of visible surface changes. We obtained the coseismic deformation created by Sivrice earthquake, which is also the first image of an earthquake captured by SAR interferometry within the EAF zone. Revealing the earthquake source characteristics in this zone is encouraging in estimating the earthquake generation capacity of the regional active faults and evaluating their potential hazard.

For the InSAR part we utilize the European Space Agency's Envisat satellite data from both ascending and descending orbital tracks to produce a coseismic surface deformation maps of the earthquake. Next, we use the interferograms to compute the optimal fault geometry through modeling the surface displacements with dislocations on fault patches embedded in an elastic half space. Consequently, we compare the relocated seismicity following the main shock with the final slip model derived from the InSAR data. We assess our results in the light of understanding the on-going tectonic regime in the region. Finally we discuss the advantages of estimating earthquake parameters based on seismicity, field observations and InSAR data when there are no apparent rupture or fissures on the surface, and improvements on the seismic moment tensor solutions obtained from seismology.

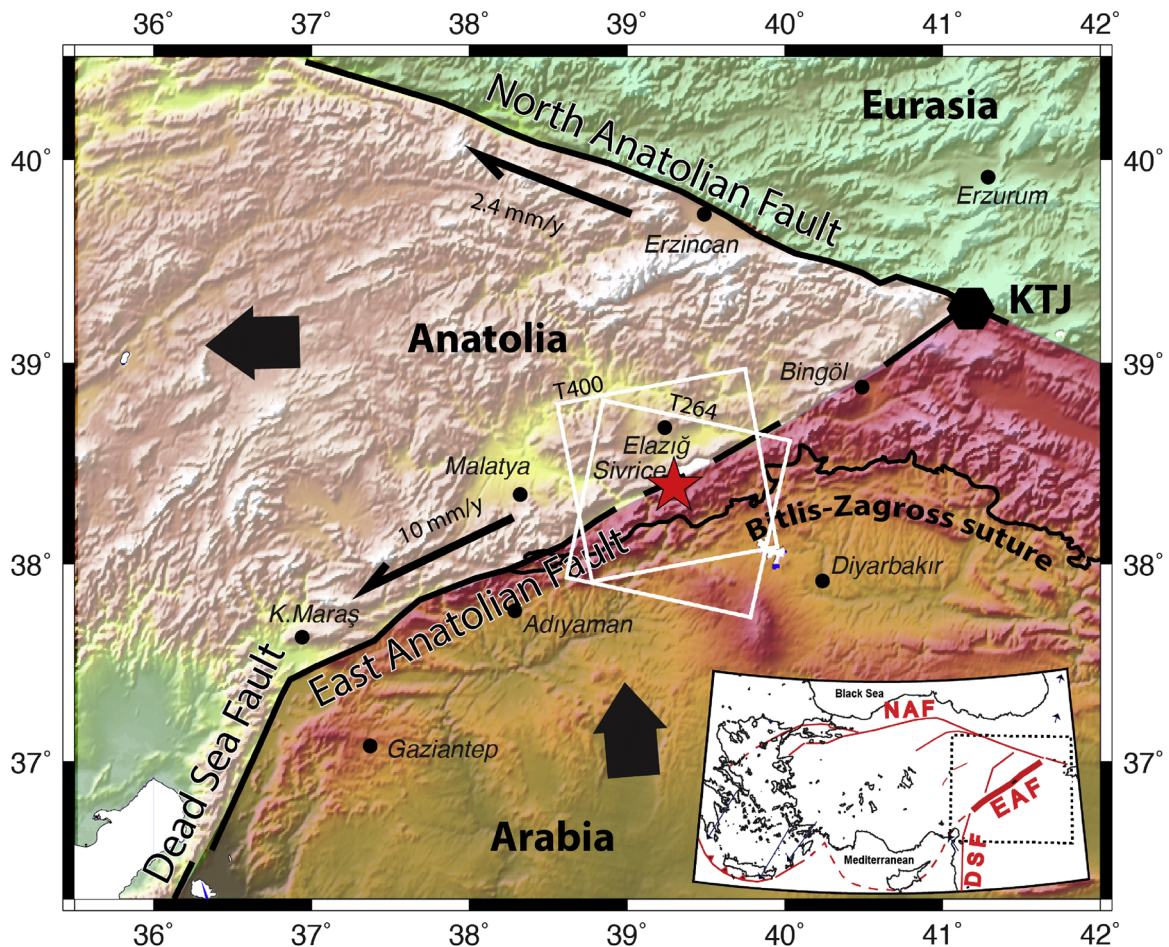


Fig. 1. Map of southeastern Turkey. The tectonic setting is governed by the westward motion of the Anatolian plate on the collisional zone where the Arabian, Eurasian and Anatolian plates come together at the Karliova triple junction (KTJ). The dextral North Anatolian and sinistral East Anatolian strike-slip faults accommodate the Anatolian plate's tectonic escape from the collision of Arabian and Eurasian plates that is delineated by the diffuse Bitlis-Zagros suture zone. Black and thick arrows show the motions of Anatolia and Arabia with respect to Eurasia. The thin solid arrows are the slip rates of 10 mm/yr for the East Anatolian Fault and 24 mm/yr for the North Anatolian Fault relative to the Arabian and Eurasian plates respectively (Reilinger et al., 2006). The red star shows the location of the Mw 5.7 February 21, 2007 Sivrice earthquake. The white boxes represent the ENVISAT ASAR frames from tracks T264 and T400, while the shaded topography is from Shuttle Radar Topography Mission (SRTM) 90 m – posting data. The inset map in the lower right corner shows the main tectonic structures of Turkey and surrounding area (the major faults are given in solid red colored lines). (For interpretation of the references to color in this figure legend, the reader is referred to the web version of this article.)

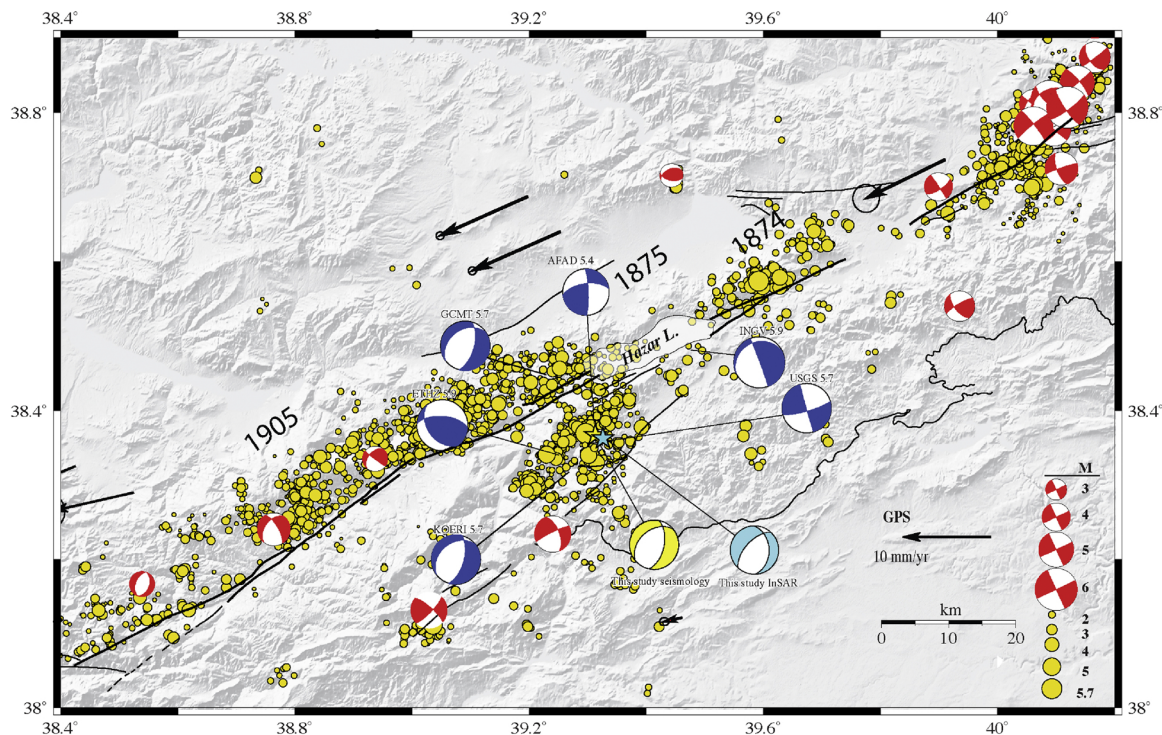


Fig. 2. Map of 5-year seismicity following the Mw 5.7 February 21, 2007 Sivrice earthquake. Black lines are the mapped active faults (Emre et al., 2013). The locations of the major historical earthquakes are indicated with their year of occurrences. The black solid arrows are the GPS velocity vectors in reference to the Arabian Plate (Reilinger et al., 2006). The red beachballs are the focal mechanism solutions of earthquakes taken from (TUBITAK TURDEP Project (105G019), 2007). The blue beachballs are the solutions of the 2007 Sivrice earthquake by different research groups/institutions listed in Table 1. The beachballs in light blue (InSAR data) and yellow (seismology) are the focal mechanisms determined in this study. The shaded topography is from SRTM data. (For interpretation of the references to color in this figure legend, the reader is referred to the web version of this article.)

2. Seismotectonic setting

The main tectonic structures in the Eastern Mediterranean are the North and East Anatolian transform faults, along with the Dead Sea fault and the Hellenic arc. The EAF forms the boundary between the Anatolian and Arabian plates. This fault was first described by Allen (Allen, 1969). Later, Arpat and Şaroğlu named the fault and mapped its strike direction (Arpat and Şaroğlu, 1972). The EAF is a long, sinistral strike-slip fault zone between the Karlıova triple junction (KTJ) in the northeast and the Dead Sea fault (DSF) in the southwest (Fig. 1). With reference to Arabia, GPS measurements indicate a governing sinistral strike-slip of around 10–11 mm/yr rate in the EAF zone (McClusky et al., 2000; Çetin et al., 2003; Reilinger et al., 2006) (Fig. 2). Together with the North Anatolian fault (NAF), its dextral strike-slip conjugate, they house the most pronounced neotectonic element of Turkey – the westward motion of the Anatolian plate from the collision zone between Arabia and Eurasia into the Hellenic subduction zone (McKenzie, 1972; Dewey and Şengör, 1979; Jackson and McKenzie, 1988; Karabulut et al., 2019). Historically, both faults have produced destructive earthquakes. The NAF, in the last century, produced eight large, greater than Mw 7 earthquakes and caused significant property damage with more than 60,000 fatalities (Ambraseys and Finkel, 1995; Barka, 1996). Over the same period of time, the EAF has been seismically less active, characterized by small to medium sized earthquakes. The largest earthquake (Mw 6.7) in the instrumental period is the 1971 Bingöl earthquake. It caused casualties between 755 (Arpat and Şaroğlu, 1972) and 878 (Ellul et al., 2004), with broad property damage. Still, the EAF was depicted with relatively infrequent, yet significant earthquakes as documented by the pre-instrumental period records (Ambraseys, 1989).

In the past, only earthquakes with large fault ruptures, or extensive

damages grabbed the attention of the chroniclers. Typically, locations of the historical earthquake are inferred from the reported coverage and degrees of damage in the age-old settled areas. We contend that a big deal of the historical records are evasive as the exact location, extent of the rupture are obscure and admittedly “hard to verify” (Ambraseys and Finkel, 1995). There are three significant historical earthquakes attributed to the region around Sivrice (Fig. 2). Excluding the 1874 normal faulting earthquake on the Gezin fault (GF) (Çetin et al., 2003; Ambraseys, 2009), which is claimed to be the reason for Hazar Lake’s southeastern outlet uplift, the locations of the other two are not accurately known due to their widespread effects.

Sivrice is raised on nutrient-rich alluvial deposits washed down by streams and snowmelt from the surrounding steep mountain slopes. Its proximity to fresh water has also been attracting dwellers for centuries. Under these circumstances, Sivrice county was and is still in our day susceptible to recurring losses at every significant earthquake not only on the EAF but also on any nearby active faults. Koçiyiğit and Aksoy documented some active, parallel or sub-parallel neighboring faults as the Elazığ, Uluova, Adıyaman, and Lice-Cemik (Koçiyiğit et al., 2003; Aksoy et al., 2007). Among these, the AF is the most prominent and longest EAF splay, which is located south of the tectonic depression of Hazar Lake. According to Şengör, it initiated coevally with the East Anatolian fault in Late Miocene–Early Pliocene (Şengör et al., 1985). The AF trends in N65°E direction and extends over 75 km from Palu to the city of Adıyaman with a clear expression in the topography (Khalifa et al., 2018). The existence and activity of the AF zone is studied and found through offsets on the Caru and the Maden streams, including the Euphrates River drainage system. Further, in consort with the offsets there are relatively young pull-apart basin formations, as well as “linear to steeply sloping fault scarps” (Çolak et al., 2012).

3. Relocated aftershocks and seismicity

We reprocessed the seismicity between the years, 2007 and 2012 using the catalogs of the General Directorate of Disaster Affairs of Turkey (AFAD), and Kandilli Observatory & Earthquake Research Institute (KOERI). For the earthquakes that exist in both catalogs (AFAD and KOERI), phase readings were merged. The earthquakes that existed only in one of the catalogs were also included in the joint catalog. A supplementary data source was the seismicity archive of TUBITAK TURDEP Project (105G019) that commenced in 2007, and which had accomplished the highest-resolution seismic observations in the region. We constructed a waveform database based on the merged catalogs and revised the phase pickings using the continuous waveforms. The final presented catalog contains 5950 events between January 01, 2007 and April 30, 2012.

We relocated the earthquakes using the HYPOCENTER program (Lienert et al., 1986). A 1-D velocity model was computed using the VELEST inversion code which minimizes travel time errors (Kissling et al., 1994). The deviations from the 1-D velocity model were accounted for the station corrections. The mean horizontal uncertainties are ~ 2.0 km and the mean of the depth uncertainties is ~ 3 km. The magnitude completeness of the catalog is ~ 2.7 . We further improved locations using the HypoDD software (Waldhauser and Ellsworth, 2000; Waldhauser, 2001), which utilizes a “Double-Difference” algorithm. The distribution of relocated aftershocks during 6 months following the main shock, and later extended to seismicity of 5 years between 2007 and 2012, suggests that a fault with a NE–SW strike between the Adiyaman and the EAF ruptured during the earthquake, which refers to the location of the AF (Fig. 2).

4. InSAR analysis

It is worthwhile to note that in the area of eastern Anatolia, the Sivrice earthquake is the first one detected by a space-borne SAR and successfully imaged using InSAR techniques. Because of its matchless potential, InSAR is extensively used in studying crustal deformations caused by earthquakes (Massonnet et al., 1993; Zebker et al., 1994; Massonnet and Feigl, 1998; Bürgmann et al., 2000; Wright et al., 2001; Funning et al., 2005; Çakır and Akoğlu, 2008). To construct the coseismic interferograms, two pairs of SAR images were taken from the ascending track T400 and a single one from the descending orbital track of T264. The images span the time frame between May 21, 2005, and March 10, 2008.

We removed the topographic contributions to the radar phase utilizing a simulation of a digital elevation model (DEM) from SRTM void filled data (Farr et al., 2007). After isolating the orbital and topographic effects from the interferometric phase we obtained the line-of-sight (LOS) component of the surface deformation that occurred within the bounds of the SAR data acquisition times (Gabriel et al., 1989). Usually, the coherence or the quality of fringes in an interferogram tends to diminish with extending the time duration between image acquisitions, which is known as the temporal baseline. In spite of the two years outpacing temporal baselines, the epicenter of the Sivrice earthquake was adequately captured and mapped by InSAR. The deformation is self-evident in the entire data set comprising three interferogram-pairs, which are available for this work (Table 2).

Table 2

Coseismic pairs of SAR images from descending and ascending orbit tracks processed in this study.

IFG	Track #	Frame #	Orbit #1	Date #1	Orbit #2	Date #2	Δ Date	B_{\perp} (m)
Int-1	264 (Dsc)	2835	16851	20050521	28374	20070804	805	65
Int-2	400 (Asc)	2835	16987	2005053	31516	2008031	1015	84
Int-3	400 (Asc)	2835	19492	20051121	31516	20080310	840	20

In our case, the long temporal baseline certainly imprints its manifestation in the images. Nevertheless, effective regional factors as the sparse vegetation and prevailing arid climate accompanied by small spatial perpendicular baselines (20–85 m, Fig. 3a–c) favored the presence of clear coseismic fringes on each interferogram.

In order to increase the clarity of the fringes we used adaptive interferogram filtering based on the power spectrum of the fringes (Goldstein and Werner, 1998). Three concentric fringes are present in all of the interferometric images with similar signals from two different illumination look angles of the complementary ascending and descending orbital tracks (Fig. 3). The fringes crop up south of Hazar Lake and spotlight the location of the epicenter of the earthquake. Three fringes would yield a LOS deformation of around 8.5 cm in the case of ENVISAT ASAR images. Also, absence of an immediate neighboring lobe (which is typical for strike-slip faulting) on the images from both orbital tracks, T264 and T400, suggests that the deformation is predominantly vertical, associated with a vertical dip slip earthquake. We can note that in each interferogram the lobe of fringes is prominently asymmetrical with the direction of long axis matching with the AF trace and mostly confined in a region between the AF and the EAF. Aforementioned features and the geological structure of the region suggest that the earthquake is associated with a rupture on a north dipping fault. Moreover, the fringes in the interferograms manifest a weak offset right above the NE part of the AF surface trace that is reflected through the digitized fringes used further in the elastic dislocation modeling (Fig. 4).

This suggests that together with the major vertical slip there is a secondary, small-scale horizontal slip of the ruptured plane, which occurred during the main shock. As the slave images used in our work were acquired a few months after the earthquake, presumably a post-seismic dislocation also took place. Finally, in the interferogram images, we observe that the AF cuts at an angle through the southeastern edge of the fringes’ lobe. This peculiar detail is remarkably analogous with the Orta earthquake in Turkey (Çakır and Akoğlu, 2008), which suggests that the rupture took place on the AF plane with listric geometry.

5. Elastic dislocation modeling

The asymmetric single-lobe deformation, which is cut through by the AF fault trace is observed in each interferogram available for this study – on the descending track T264, and in the two pairs of images taken from the ascending track T400. This deformation is consistent with normal-slip motion on a fault that likely has listric geometry. Otherwise, the fringes should have been entirely confined to the hanging wall (*i.e.* the northern block) of the AF. To demonstrate this, we calculated a broad array of fault displacements by applying a single-fault elastic dislocation model (Okada, 1985) inferred from the InSAR data. In the interest of estimating the ruptured fault parameters, we modeled InSAR data on finite surface elements embedded in homogeneous, isotropic, elastic, flat half-spaces.

First, we used dislocations on rectangular surface elements to model the fault rupture. We inverted the SAR data set through a residual-minimization procedure based on a downhill simplex simulated annealing algorithm developed by Donnellan and Lyzenga (1998). An objective function with χ^2 fit is derived from the interferometric SAR

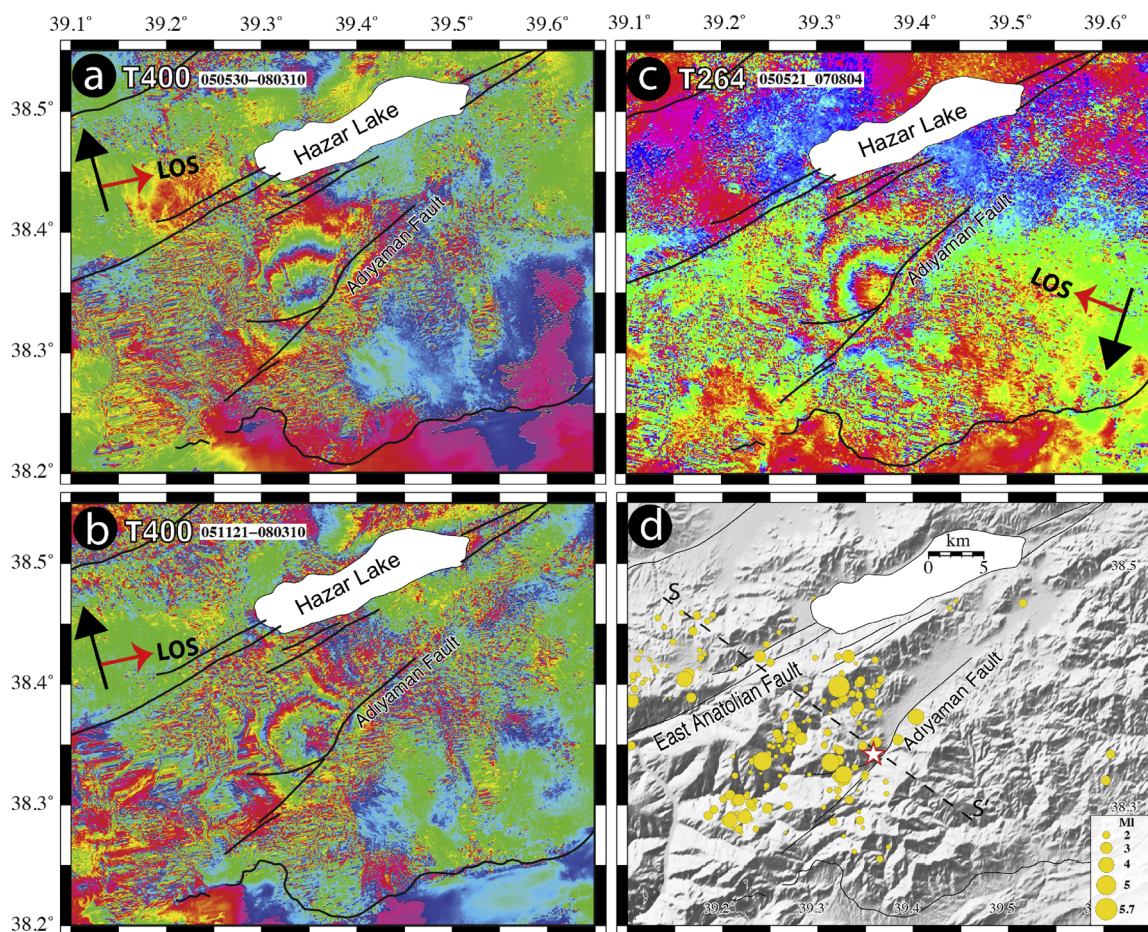


Fig. 3. (a–c) Coseismic interferograms of the Mw = 5.7, February 21, 2007 Sivrice earthquake captured in total by 3 pairs of images acquired from T400, an ascending orbital track, and T264, a descending orbital track of ENVISAT. The red and black arrows orthogonal to each other in each image show the satellite flight direction (ascending & descending) and the line of sight direction (right looking), respectively. The surface deformation due to the earthquake appears as an elliptical lobe with 3 fringes south of the Lake Hazar, revealing that the event took place ~ 9 km south of Sivrice town on the Adiyaman fault, a splay from the EAF. (d) Relocated aftershocks of the following 6 months after the main shock with the SRTM data (Fig. 1). The red star shows the location of the earthquake determined from the InSAR data in this study (see Table 1 for details). (For interpretation of the references to color in this figure legend, the reader is referred to the web version of this article.)

data batch consistent with its measurement uncertainties. Critical unwrapping errors emerged as a consequence of the high temporal decorrelation observed in the images. The unwrapping of the coseismic/wrapped data was ineffective and we modeled the wrapped phase data by digitizing the fringes. This allowed us to reduce the complexity of a large number of data points down to 530 data points, focusing in the region of interest and significantly reducing the computation time.

The inversion process solves nine parameters of a single-fault model, which are the longitude, latitude, strike, dip, depth, width, length, strike-slip and dip-slip components. To calculate the uncertainties of the fault parameters, we took far-field data where no deformation signal is present as a result of the earthquake. Using the far-field data power spectrum we calculated and radially averaged a two-dimensional autocorrelation function (Hanssen, 2001). Further, a colored noise model was fitted to the estimated one-dimensional covariance function. In order to test the robustness of the model, we used the procedures described by Fukushima (Fukushima et al., 2003), and constructed 500 simulations of spatially correlated random noise that harmonize with the colored noise model. Over similar wavelengths with the model we used the spatially correlated synthesized noise to produce 500 perturbed data sets (Funning et al., 2005). Subsequently, the perturbed data sets were inverted for nine fault parameters. In addition, we used an empirical approach defined by Wells and

Coppersmith (1994) for the moment magnitude Mw 5.7 of the earthquake. Considering that earthquake parameters demand rupture dimensions, dislocation, and moment magnitude are consistent, we disregarded slip values that were higher than 2 m and ended up with 286 out of 500 perturbed data points. The earthquake parameters uncertainties, along with their trade-offs are plotted in Fig. 5.

The obtained finite-fault model shows that the SAR data requires a fault slip with a strike direction of N42°E, dipping northward at 59°, with a rake of -73° (normal fault with left lateral strike-slip component), and it is located at a depth below 5 km, with an RMS misfit of 0.53 cm (Fig. 5). In Fig. 4b, the computed synthetic interferograms for the descending and ascending orbits are presented from the best fit single-fault model. The calculated fault parameters, including the geodetic moment, are in good agreement with seismological observations (Table 1). For each of the descending and ascending data set we employed the parameters obtained from the best fit model and estimated their residual interferograms. A visual assessment demonstrated that the best fit model successfully reproduces the main features of the observed data set.

The model fault given in Fig. 4c (i.e. the white rectangle, which is the vertical projection of the ruptured portion of the fault plane to the surface) with its location, strike and dip direction coincides well with the AF and explains the observed coseismic fringes. This is also

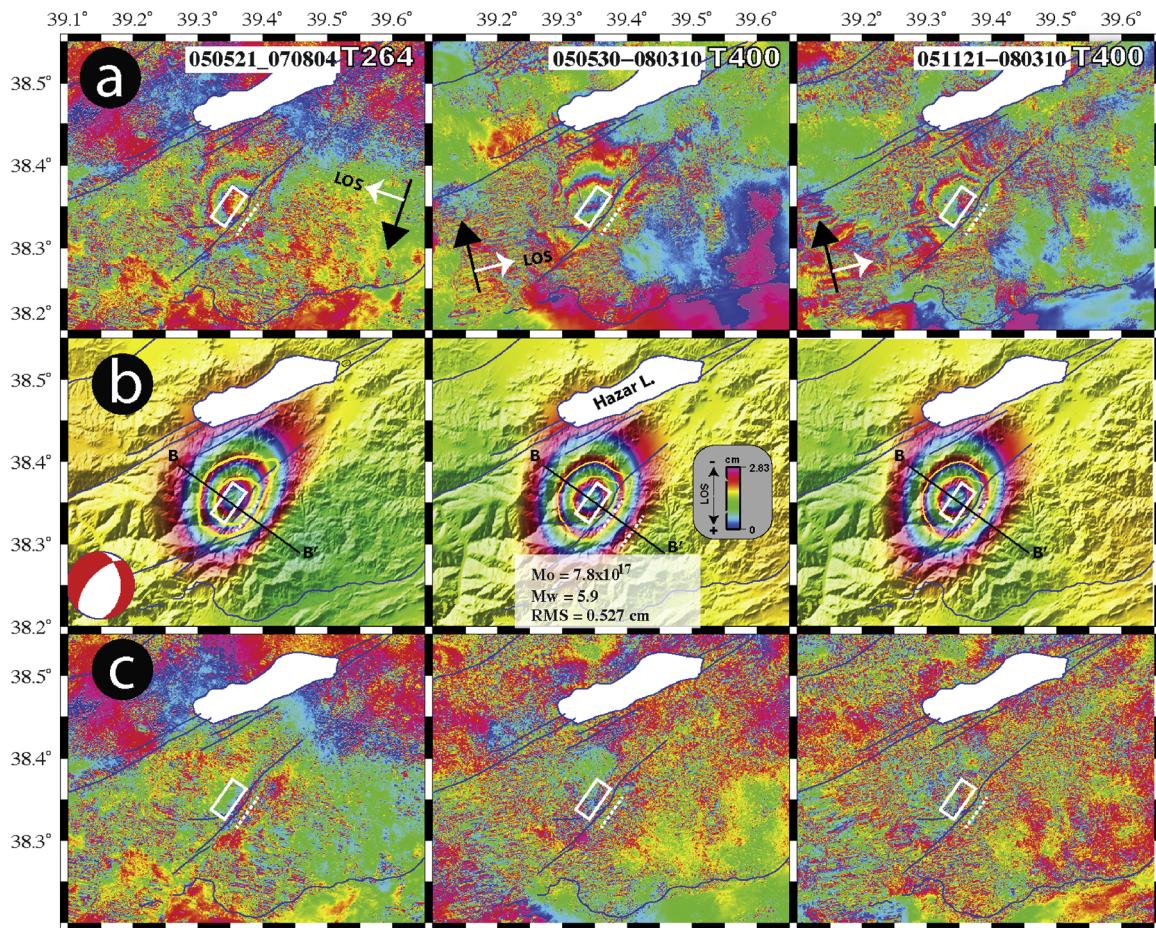


Fig. 4. Interferometric data used in this work. (a) The calculated coseismic interferograms. The white rectangle is the surface projection of the best-fit fault model. The source parameters are produced through fitting single-fault model. The first image is for the wrapped descending track T264, and the next two on the right are for the wrapped ascending T400. The black arrows indicate the direction of satellite tracks and the white arrows are the LOS vectors for each interferometric image. The dashed line is the up-dip projection of the fault on earth surface at about 3 km southeast further from the AF. (b) The synthetic interferograms produced through single fault Okada elastic dislocation model of a fault with the best-fit fault model parameters from the inversions – strike $N42^{\circ}E$, dip 59° , rake -73° , at a depth below 5 km. The continuous and enclosed yellow lines are the digitized fringes used in the inversions. B–B' is the fault perpendicular section, giving the fit between the data and the model. (c) The residual interferograms obtained by subtracting the modeled/synthetic (b) from the observed interferograms (a). (For interpretation of the references to color in this figure legend, the reader is referred to the web version of this article.)

supported and could be distinguished from the profiles given in Fig. 6a. Alternatively, we inverted the data for a SE-dipping fault. The calculated residual interferograms and the slip RMS (0.65 cm) were within the satisfactory limits. Further, the apparent distribution of seismicity, the presence of a seismic gap between the AF and the EAF in Fig. 6b, and the geological structure in the region favor the NW dipping rupture direction.

The relationship between the fault model at depth and the AF at the surface is comparable to the observation of the 2000 Orta earthquake (Çakır and Akoğlu, 2008). Likewise, the model suggests that the dip values of the AF change nearly down from 90° at the surface, to about 59° at depths of around 5 km. A specific concern, pertaining to the case of a flat planar fault model, is the up-dip surface projection, which would have been at earth surface further southeast from the AF (Fig. 4c – the white dashed line). This is a mountainous area with no apparent fault morphology as seen in Fig. 3d. Hence, our fault model requires a decrease in its dip angle values, as the only nearby geomorphological expression to which the rupture could be assigned to is the AF (Fig. 4). This inference is supported by the fact that each of the lobes of fringes in the observed data set of descending or ascending wrapped images are also cut through by the AF. Therefore, the AF connects to the ruptured fault plane at depth by retaining a listric geometry as shown in Fig. 6b.

The AF reactivation view is also strengthened by the expressed discontinuities in the fringes matching up with the map expression of the fault.

For the last phase of modeling we constructed a listric fault using finite triangular surface elements (Fig. 7). We inverted the modeled coseismic slip using the Poly3Dinv software (Thomas, 1993; Maerten et al., 2005), which computes the quasi-static displacement, strain and stress fields. In our case, we undertook the ruptured surface in two distinct parts. The bottom part of the listric fault exemplifies the planar fault attained from the best fit single fault model shown in Fig. 4. This solution did not enhance the data fit and produced a similar misfit value of $RMS = 0.5$ cm. The primary reason is that the listric fault surface does not overlay one-to-one the best fit single-fault planar model and inverting it linearly fails to improve the data fit.

The Poly3Dinv solution resulted in a coseismic slip on the lower section of the fault. Moreover, the variable slip model predicted a peak slip of 1.5 m in the center of the lobe. The slip amplitude is a function of a smoothing, which is a setup parameter given prior to the modeling process. The smoothing parameter varies between zero with no smoothing, and one. Therefore, the smoother the parameter is, the lower values of the slip are attained. In our case, we took a smoothing factor of 0.2.

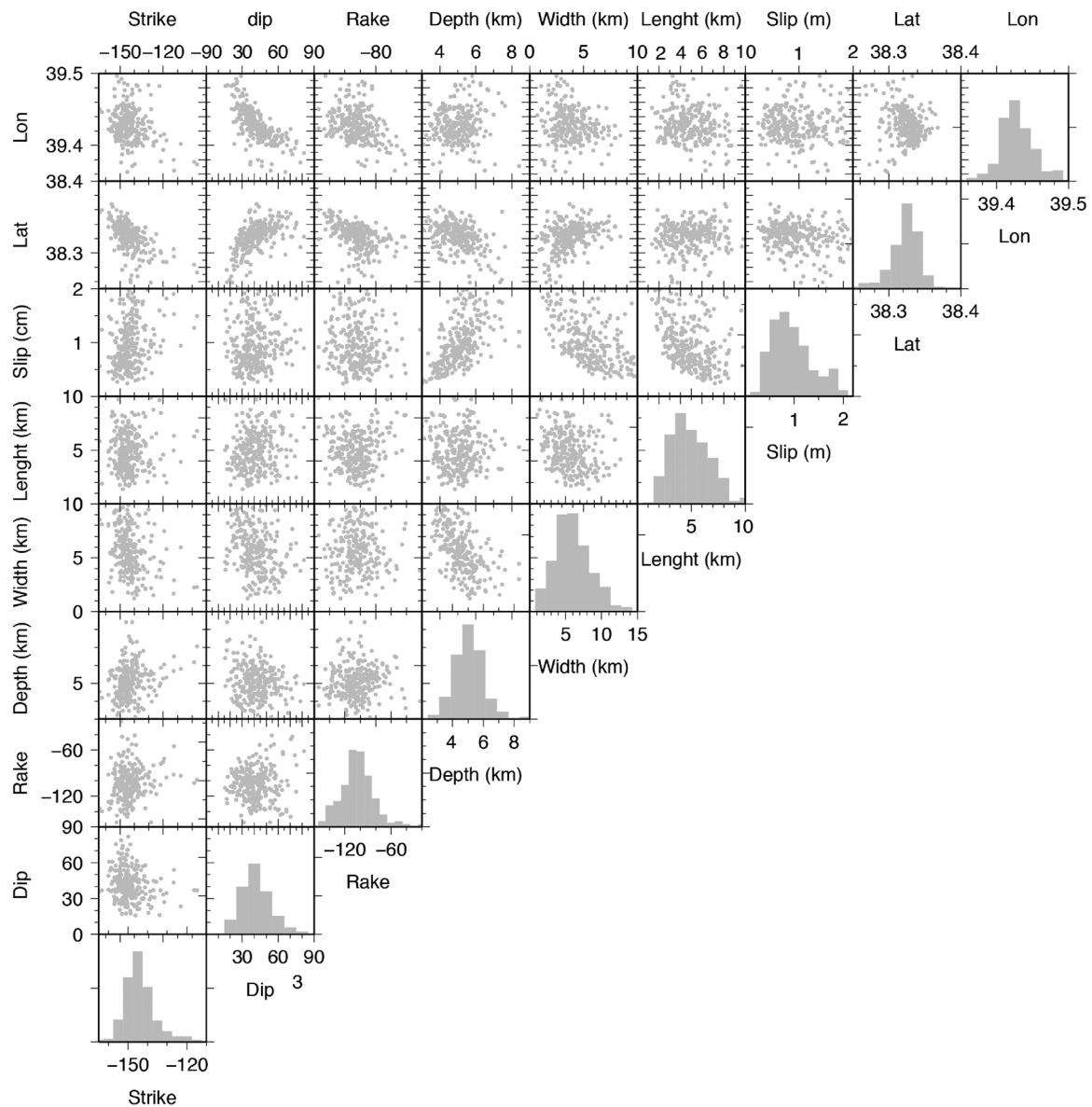


Fig. 5. Uncertainties and trade-offs in model parameters for a single fault model. The histograms give the degree of uncertainty for each model parameter. The scatterplots illustrate the correlation or the trade-offs measure between the model parameters in pairs.

6. Discussion and conclusion

In this study, we described coseismic displacement with relocated seismicity of the 21 February 2007 Sivrice earthquake. The earthquake deformation field maps were generated using InSAR data from descending and ascending orbital tracks of ENVISAT ASAR. The InSAR observations and the elastic dislocation slip models suggest that the earthquake was dominated by normal faulting with left-lateral strike-slip component on the Adıyaman fault with a listric geometry. The slip vector orientations obtained from the models are plotted on a rose diagram indicating that the azimuth dominates in a direction of N65°W (Fig. 8). The results are consistent with the left-lateral strike-slip shear regime of the region (the inset in the upper left corner of Fig. 8).

As the ruptured fault segment does not project to the surface at the trace of the AF, we consider the three possibilities: (1) the fault is listric, (2) the earthquake ruptured a fault structurally beneath the AF, which outcrops further southeast, and (3) the ruptured fault intersects the AF at depth (blind fault).

The first model is supported by the seismicity pattern, which in the

lower part of the ruptured plane suggest listric geometry, while the upper portion (depth less than 4 km) appear to be distributed over a more steep plane. The presence of an immediate concave bow shaped fault trace on the map view (Fig. 3), characteristic to listric faults, also supports this idea. The neighboring triangular mountain facets in the NE imply that there is an insular (on a local scale) system of normal faulting.

The second model, a rupture on a fault that outcrops further southeast is opposed by the structural properties of the regional geology, unless it is a fault with significantly low slip rate.

The third model assumes the presence of a blind fault that cuts the AF at depth. The coseismic interferograms acquired from two different look angles carry the same signal, which indicates a normal fault rupture. Also, as the best fit single-fault model is a fracture with an upper bound of less than 4 km, we would have expected the topography just over the fracture to change accordingly. However, as we do not observe the change, we assume that the listric faulting is superimposed on an interlace of complex faulting. A future study could be based on elaborating this particular fact.

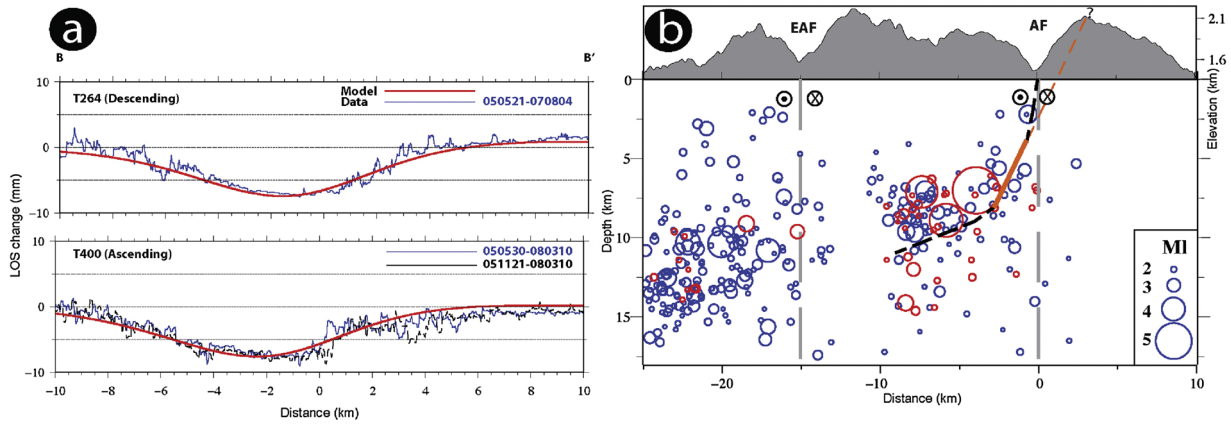


Fig. 6. (a) Data fit between the observed and the model. (b) Seismicity depth distribution of 5-year (the blue circles) and 6-month (the red circles) relocated seismic data following the main shock. The thick red line is the modeled fault plane inferred from the inversion using a simulating annealing algorithm. The up-dip projection of the ruptured plane during the earthquake (the question mark “?” location) does not correspond to the surface trace of the Adiyaman Fault (AF). Hereby, the location of the earthquake rupture and its mode of transmission with respect to the Adiyaman surface trace suggest that it has listric geometry. The grey shaded area represents the topography of the region. (For interpretation of the references to color in this figure legend, the reader is referred to the web version of this article.)

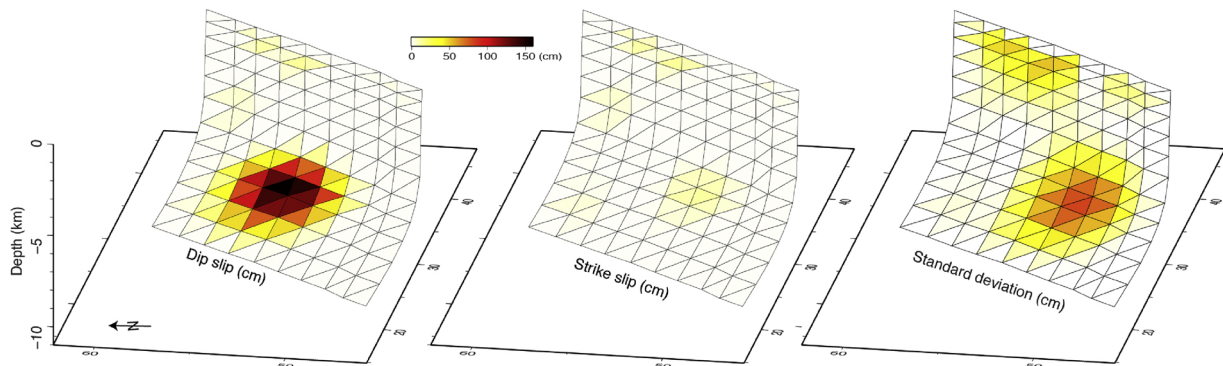


Fig. 7. Slip distribution of the Sivrice earthquake on a listric fault plane constructed with triangular elements obtained using the Poly3Dinv software (Maerten et al., 2005). The curvilinear fault surface encompasses the single fault predicted by the Simplex inversion. The dip slip varies along the fault up to 1.5 m, at depths between 5 and 10 km. The strike component of the total slip is relatively small of max ~ 20 cm. The resilience of our model to noise and the uncertainty of the slip distribution with depth is achieved through inversions of 500 InSAR data sets perturbed with synthetic noise.

The listric faults in this region may have been originated from thrust faults that later had been reactivated under the geometric constraints of the present-day regime. Evidently, the presence of a nearby and well-defined tectonic depression of Hazar Lake highlights that some parts of the EAF zone undergo extensional phases. About 6 km south of Hazar Lake another extensional crustal unit, the plain of Bermaz, is located and is cut through by the AF in NE–SW direction. In a study by Aksoy et al. (2007) described Hazar Lake as a negative flower formation, with a splay of subsidiary faults including normal vertical components. In other words, the listric faults found inward from southern shore of the lake exhibit a “step-like morphology” firmly signifying extension, which is normal faulting (Aksoy et al., 2007). This morphology can be produced either by the presence of geometric constraints or depth variations of the rheology. Such as ongoing extensional stresses are able to reactivate old curved thrusts (*i.e.* negative tectonic inversion), or rather faults may curve so as to accommodate rotational deformations (Jackson and McKenzie, 1983). The former is the most likely scenario in our case as prior or during the formation of the EAF the continental collision between the Arabian and Anatolian plates must have created widespread splays of thrust faults with varying shape and geometry along the Bitlis-Zagros suture. Reactivation of faults over different deformation phases has been described for many tectonic settings

worldwide (Wernicke, 1981; Wernicke and Burchfiel, 1982; Williams et al., 1989; Gautier and Brun, 1994). The Apennines is one of the best-documented examples of negative inversion of active extension, which is developing on a compressional wedge (Ghiesetti and Vezzani, 1999).

Although listric faults are common, not many earthquakes associated with listric faulting are studied (Çakır and Akoğlu, 2008). There is an ample number of normal faulting earthquakes studied using both seismology and geodesy (Smith et al., 1989; Rietbrock et al., 1996; Roberts and Michetti, 2004; Friedrich et al., 2004; Chiaraluce et al., 2011; Whipp et al., 2014; Liu et al., 2017). Most of these studies assume planar faults when modeling rupture propagation or static geodetic data such as InSAR, GPS. However, identifying the fault geometry is critical in seismic hazard analysis as the stress changes, ground acceleration and shaking time produced by an earthquake on planar or listric/curved normal faults can vary (Passone and Mai, 2017). In this study, although the surface deformation of Sivrice earthquake is captured from SAR images, which have low temporal resolution, the source parameters, and the causative fault are adequately determined. Our modeling predicts a moment magnitude of 5.9 (moment of 0.76×10^{18} Nm) that is in good agreement with the seismologically estimated sizes from various sources (Table 1).

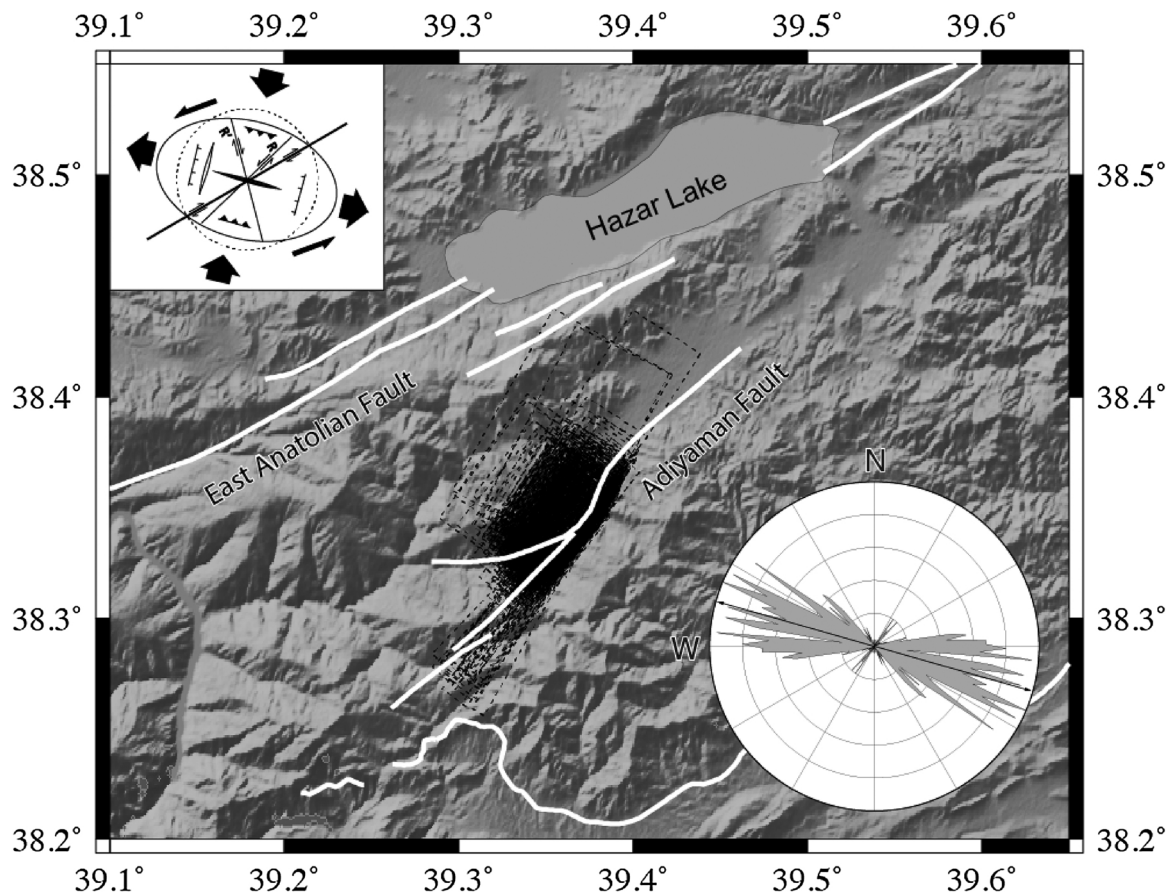


Fig. 8. Rose diagram for the predicted slip vector orientations estimated through 500 runs of inversions of the data perturbed with spatially correlated noise. The dominant azimuth direction of the slip vector orientations is N65°W plotted on the rose diagram given in the lower right corner. This direction is conforming to the left-lateral strike-slip shear regime of the East Anatolian fault region (the inset). The cluster of black dashed rectangles in the middle of figure is the surface projection of the fault planes calculated from the inversions. The shaded relief is derived from SRTM data.

Acknowledgements

This study was supported by the Scientific Council of Turkey (TUBITAK, project 114Y250). SAR data are provided by the European Space Agency (ESA) through the Geohazard Supersites and Copernicus programs. We would like to thank the anonymous reviewers for their prudent reading of our manuscript and their many insightful comments and suggestions.

Appendix A. Supplementary data

Supplementary data associated with this article can be found, in the online version, at <https://doi.org/10.1016/j.jog.2019.101654>.

References

- Aksoy, E., Inceöz, M., Koçiyigit, A., 2007. Lake Hazar basin: a negative flower structure on the East Anatolian Fault System (EAFS), SE Turkey. *Turk. J. Earth Sci.* 16, 319–338.
- Allen, C.R., 1969. Active Faulting in Northern Turkey. Division of Geological Sciences, pp. 1577.
- Ambraseys, N.N.N., 1989. Temporary seismic quiescence: SE Turkey. *Geophys. J. Int.* 96, 311–331.
- Ambraseys, N.N.N., 2009. Earthquakes in the Mediterranean and Middle East: A Multidisciplinary Study of Seismicity up to 1900.
- Ambraseys, N.N.N., Finkel, C.F., 1995. Seismicity of Turkey and adjacent areas: a historical review. *MS Eren 1500–1800*.
- Arpat, E., Şaroğlu, F., 1972. The East Anatolian fault system: thoughts on its development. *Bull. Miner. Res. Explor. Inst. Turkey* 78, 33–39.
- Barka, A.A., 1996. Slip distribution along the North Anatolian fault associated with the 695 large earthquakes of the period 1939 to 1967. *Bull. Seismol. Soc. Am.* 86, 1238–1254.
- Bürgmann, R., Rosen, P.A., Fielding, E.J., 2000. Synthetic aperture radar interferometry

- to measure Earth's surface topography and its deformation. *Annu. Rev. Earth Planet. Sci.* 28, 169–209. <https://doi.org/10.1146/annurev.earth.28.1.169>.
- Çakır, Z., Akoğlu, A.M., 2008. Synthetic aperture radar interferometry observations of the M = 6.0 Orta earthquake of 6 June 2000 (NW Turkey): reactivation of a listric fault. *Geochem. Geophys. Geosyst.* 9, Q08009. <https://doi.org/10.1029/2008GC002031>.
- Çetin, H., Güneşli, H., Mayer, L., 2003. Paleoseismology of the Palu–Lake Hazar segment of the East Anatolian fault zone, Turkey. *Tectonophysics* 374, 163–197.
- Çolak, S., Aksoy, E., Koçiyigit, A., Inceöz, M., 2012. The Palu-Uluova strike-slip basin in the East Anatolian fault system, Turkey: its transition from the Palaeotectonic to Neotectonic stage. *Turk. J. Earth Sci.* 21, 547–570.
- Chiarioluca, L., Valoroso, L., Piccinini, D., Di Stefano, R., De Gori, P., 2011. The anatomy of the 2009 L'Aquila normal fault system (central Italy) imaged by high resolution foreshock and aftershock locations. *J. Geophys. Res.: Solid Earth* 116, B12.
- Dewey, J.F., Şengör, A.C., 1979. Aegean and surrounding regions: complex multiple and continuum tectonics in a convergent zone. *Geol. Soc. Am. Bull.* 90, 84–92. <https://doi.org/10.1130/0016-7606>.
- Donnellan, A., Lyzenga, G.A., 1998. GPS observations of fault afterslip and upper crustal deformation following the Northridge earthquake. *J. Geophys. Res.* 103, 21285–21297. <https://doi.org/10.1029/98JB01487>.
- Ekström, G., Nettles, M., Dziewonski, A.M., 2012. The global CMT project 2004–2010: centroid-moment tensors for 13,017 earthquakes. *Phys. Earth Planet. Inter.* 200–201, 1–9. <https://doi.org/10.1016/j.pepi.2012.04.002>.
- Ellul, F., D'Ayala, D., Calayir, Y., 2004. The 1st of May 2003, Bingol, Turkey, earthquake, a study of the performance of the building stock. In: *Proceedings of the 13th World Conference of Earthquake Engineering*. University of Bath.
- Emre, Ö., Duman, T.Y., Özalp, S., Elmaci, H., Olgun, S., Şaroğlu, F., 2013. Active Fault Map of Turkey with an Explanatory Text. General Directorate of Mineral Research and Exploration, Special Publication Series, 30.
- Farr, T.G., Rosen, P.A., Caro, E., Crippen, R., Duren, R., Hensley, S., Kobrick, M., Paller, M., Rodriguez, E., Roth, L., 2007. The shuttle radar topography mission. *Rev. Geophys.* 45, RG2004. <https://doi.org/10.1029/2005RG000183>.
- Friedrich, A.M., Lee, J., Wernicke, B.P., Sieh, K., 2004. Geologic context of geodetic data across a Basin and Range normal fault, Crescent Valley, Nevada. *Tectonics* 23, 2.
- Fukushima, Y., Nishizawa, O., Sato, H., Ohtake, M., 2003. Laboratory study on scattering characteristics of shear waves in rock samples. *Bull. Seismol. Soc. Am.* 93, 253–263.
- Funning, G.J., Parsons, B., Wright, T.J., Jackson, J.A., Fielding, E.J., 2005. Surface displacements and source parameters of the 2003 Bam (Iran) earthquake from Envisat

- advanced synthetic aperture radar imagery. *J. Geophys. Res.: Solid Earth* 110, 89. <https://doi.org/10.1029/2004JB003338>.
- Gabriel, A.K., Goldstein, R.M., Zebker, H.A., 1989. Mapping small elevation changes over large areas: differential radar interferometry. *J. Geophys. Res.: Solid Earth* 94, 9183–9191.
- Gautier, P., Brun, J.P., 1994. Crustal-scale geometry and kinematics of late-orogenic extension in the central Aegean [Cyclades and Ewia Island]. *Tectonophysics* 238, 399–424.
- Ghiesetti, F., Vezzani, L., 1999. Depths and modes of crustal extension of the Apennines [Italy]. *Terra Nova* 11, 67–72.
- Goldstein, R.M., Werner, C.L., 1988. Radar interferogram filtering for geophysical applications. *Geophys. Res. Lett.* 25, 4035–4038.
- Hanssen, R.F., 2001. *Radar Interferometry: Data Interpretation and Error Analysis*, vol. 2 Springer Science & Business Media.
- Jackson, J.A., McKenzie, D.P., 1983. The geometrical evolution of normal fault systems. *J. Struct. Geol.* 5, 471–482. [https://doi.org/10.1016/0191-8141\(83\)90053-6](https://doi.org/10.1016/0191-8141(83)90053-6).
- Jackson, J.A., McKenzie, D.P., 1988. The relationship between plate motions and seismic moment tensors, and the rates of active deformation in the Mediterranean and Middle East. *Geophys. J. R. Astron. Soc.* 93, 45–73.
- Karabulut, H., Paul, A., Ozbakir, A.D., Ergun, T., Senturk, S., 2019. A new crustal model of the Anatolia-Aegean domain: evidence for the dominant role of isostasy in the support of the Anatolian plateau. *Geophys. J. Int.* 218, 57–73.
- Khalifa, A., Çakır, Z., Owen, L., Kaya, Ş., 2018. Morphotectonic analysis of the East Anatolian Fault, Turkey. *Turk. J. Earth Sci.* 27, 110–126.
- Kissling, E., Ellsworth, W.L., Eberhart-Phillips, D., Kradolfer, U., 1994. Initial reference models in local earthquake tomography. *J. Geophys. Res.* 99, 19635–19646. <https://doi.org/10.1029/93JB03138>.
- Koçyiğit, A., Aksoy, E., İnceöz, M., 2003. Basic Neotectonic Characteristics of the Sivrice Fault Zone in the Sivrice-Palu Area, East Anatolian Fault System [EAFS], Turkey, vol. 20. International Workshop on the North Anatolian, East Anatolian and Dead Sea Fault Systems: Recent Progress in Tectonics and Palaeoseismology.
- Lienert, B.R., Berg, E., Neil Frazer, L., 1986. Hypocenter: an earthquake location method using centered, scaled, and adaptively damped least squares. *Bull. Seismol. Soc. Am.* 76, 771–783.
- Liu, G., Qiao, X., Xiong, W., Zhou, Y., Nie, Z., Xia, C., 2017. Source models for the 2016 Mw 6.0 Hutubi earthquake, Xinjiang, China: a possible reverse event. *Geodesy Geodyn.* 8, 311–318.
- Maerten, F., Resor, P., Pollard, D., Maerten, L., 2005. Inverting for slip on three-dimensional fault surfaces using angular dislocations. *Bull. Seismol. Soc. Am.* 95, 1654–1665. <https://doi.org/10.1785/012003018>.
- Massonnet, D., Feigl, K.L., 1998. Radar interferometry and its application to changes in the earth's surface. *Rev. Geophys.* 36, 441–500. <https://doi.org/10.1029/97RG03139>.
- Massonnet, D., Rossi, M., Carmona, C., Adragna, F., Peltzer, G., Feigl, K., Rabaute, T., 1993. The displacement field of the Landers earthquake mapped by radar interferometry. *Nature* 364, 138.
- McClusky, S., Balassanian, S., Barka, A.A., Demir, C., Ergintav, S., Georgiev, I., Gurkan, O., Hamburger, M., Hurst, K., Kahle, H., Kastens, K., 2000. Global Positioning System constraints on plate kinematics and dynamics in the eastern Mediterranean and Caucasus. *J. Geophys. Res.: Solid Earth* 105, 5695–5719.
- McKenzie, D.P., 1972. Active tectonics of the Mediterranean region. *Geophys. J. Int.* 30, 109–185. <https://doi.org/10.1111/j.1365-246X.1972.tb02351.x>.
- Okada, Y., 1985. Surface deformation due to shear and tensile faults in a half-space. *Bull. Seismol. Soc. Am.* 75, 1135–1154.
- Passone, L.P., Mai, M., 2017. Kinematic earthquake ground-motion simulations on listric normal faults. *Bull. Seismol. Soc. Am.* 107, 2980–2993. <https://doi.org/10.1785/0120170111>.
- Reilinger, R., McClusky, S., Vernant, P., Lawrence, S., Ergintav, S., Cakmak, R., Ozener, H., Kadirov, F., Guliev, I., Stepanyan, R., Nadariya, M., 2006. GPS constraints on continental deformation in the Africa–Arabia–Eurasia continental collision zone and implications for the dynamics of plate interactions. *J. Geophys. Res.: Solid Earth* 111, B5.
- Rietbrock, A., Tiberi, C., Scherbaum, F., Lyon-Caen, H., 1996. Seismic slip on a low angle normal fault in the Gulf of Corinth: evidence from high-resolution cluster analysis of microearthquakes. *Geophys. Res. Lett.* 23, 1817–1820.
- Roberts, G.P., Michetti, A.M., 2004. Spatial and temporal variations in growth rates along active normal fault systems: an example from The Lazio-Abruzzo Apennines, central Italy. *J. Struct. Geol.* 26, 339–376.
- Şengör, A.M.C., 1979. The North Anatolian transform fault: its age, offset and tectonic significance. *J. Geol. Soc.* 136, 269–282.
- Şengör, A.M.C., Görür, N., Saroglu, F., 1985. Strike-slip faulting and related basin formation in zones of tectonic escape: Turkey as a case study, in *Strike-Slip Deformation, Basin Formation, and Sedimentation*. Spec. Publ. Soc. Econ. Paleontol. Mineral. 37, 227–262.
- Smith, R.B., Reilinger, R.E., Meertens, C.M., Hollis, J.R., Holdahl, S.R., Dzurisin, D., Gross, W.K., Klinge, E.E., 1989. What's moving at Yellowstone? The 1987 crustal deformation survey from GPS, leveling, precision gravity, and trilateration. *Eos Trans. Am. Geophys. Union* 70, 113–125.
- Tepeğür, E., Yaman, M., 2007. 21 February 2007 Sivrice (Elazığ) Earthquake Report. The Turkish Ministry of Public Works and Settlement. General Directorate of Disaster Affairs, Seismology Research Department, 5690-1, pp. 1–33.
- Thomas, A.L., 1993. Poly3D: A Three-Dimensional, Polygonal Element, Displacement Discontinuity Boundary Element Computer Program with Applications to Fractures, Faults, and Cavities in the Earth's Crust. Stanford Univ., Stanford, CA.
- Waldhauser, F., 2001. hypoDD-A program to compute double-difference hypocenter locations [hypoDD version 1.0-03/2001]. *US Geol. Surv. Open File Rep.* 1, 113.
- Waldhauser, F., Ellsworth, W.L., 2000. A double-difference earthquake location algorithm: method and application to the northern Hayward Fault, CA. *Bull. Seismol. Soc. Am.* 90, 1353–1368.
- Wells, D.L., Coppersmith, K.J., 1994. New empirical relationships among magnitude, rupture length, rupture width, rupture area, and surface displacement. *Bull. Seismol. Soc. Am.* 84, 974–1002.
- Wernicke, B., 1981. Low-angle normal faults in the Basin and Range Province: nappe tectonics in an extending orogen. *Nature* 291, 645.
- Wernicke, B., Burchfiel, B.C., 1982. Modes of extensional tectonics. *J. Struct. Geol.* 4, 105–115.
- Whipp, P.S., Jackson, C.A.L., Gawthorpe, R.L., Dreyer, T., Quinn, D., 2014. Normal fault array evolution above a reactivated rift fabric: a subsurface example from the northern Horda Platform, Norwegian North Sea. *Basin Res.* 26, 523–549.
- Williams, G.D., Powell, C.M., Cooper, M.A., 1989. Geometry and kinematics of inversion tectonics. *Geol. Soc. Lond.* 44, 3–15. <https://doi.org/10.1144/GSL.SP.1989.044.01.02>. Special Publications.
- Wright, T., Parsons, B.E., Jackson, J.A., Haynes, M., Fielding, E.J., England, P.C., Clarke, P.J., 1999. Source parameters of the 1 October 1995 Dinar (Turkey) earthquake from SAR interferometry and seismic bodywave modelling. *Earth Planet. Sci. Lett.* 172, 23–37.
- Wright, T., Parsons, B., Fielding, E., 2001. Measurement of interseismic strain accumulation across the North Anatolian Fault by satellite radar interferometry. *Geophys. Res. Lett.* 28, 2117–2120.
- Zebker, H.A., Rosen, P.A., Goldstein, R.M., Gabriel, A., Werner, C.L., 1994. On the derivation of coseismic displacement fields using differential radar interferometry: the Landers earthquake. *J. Geophys. Res.* 99, 19617–19634. <https://doi.org/10.1029/94JB01179>.